

## A note on notch shape optimization to minimize stress concentration effects



Jaime Tupiassú Pinho de Castro<sup>\*</sup>, Daniel de Albuquerque Simões, Ivan Fabio Mota de Menezes, Marco Antonio Meggiolaro, Luiz Fernando Martha

Pontifical Catholic University of Rio de Janeiro, PUC-Rio, Rua Marquês de São Vicente 225, Rio de Janeiro, RJ 22451-900, Brazil

### ARTICLE INFO

#### Article history:

Received 10 February 2016  
Revised 17 March 2016  
Accepted 18 March 2016  
Available online 23 March 2016

#### Keywords:

Stress concentration effects  
Notch shape optimization  
Multiaxial loads

### ABSTRACT

Notches induce localized stress concentration effects that can affect many failure mechanisms, in particular the initiation and growth of short cracks under fatigue loads, significantly reducing the strength of structural components under service loads. To decrease such nocive effects, notches are usually designed with as large as possible circular arc tips, even though it has long been recognized this is not the best solution to minimize such problems. Indeed, notches with properly shaped variable tip radii can have a much smaller deleterious influence on fatigue strength, but such optimized notches still are not routinely used in structural design. In fact, not even standard fatigue specimens specify them. Nevertheless, such improved notches can be a very good design option to augment the strength of structural components, since they barely affect their global dimensions or weight. Moreover, nowadays they can be economically built due to the widespread availability of CNC machine tools. After comparing the improvements achievable by some classic variable radii receipts, two simple and robust numerical routines developed to optimize notch shapes for components that work under general multiaxial loading conditions are presented and evaluated.

© 2016 Elsevier Ltd. All rights reserved.

### 1. Introduction

Most structural components must have brusque geometric transition details such as holes, slots, grooves, corners, shoulders, keyways, splines, threads, welded joints, or similar localized undercuts or even reinforcements, which can be generically called notches. Such notches are usually required for operational, structural, or manufacturing reasons, or else to decrease weight, so they are in fact a practical need. However, if not properly designed they can much perturb the local stress and strain fields around them, locally increasing or concentrating the nominal stresses that would otherwise act at their sites if their effects were negligible. Such localized stress concentration effects depend on the notch geometry and on the loading conditions, and can much decrease the actual component strength. Under higher loads they depend as well on the load level and on the material hardening behavior, since local yielding and other non-linear deformation mechanisms affect the notch tip stresses and the stress gradients around them.

In simple yet very common linear elastic (LE) problems, local effects on notch-tip stresses can be quantified by a material-independent stress concentration factor (SCF) defined by

$$K_t = \sigma_{max} / \sigma_n \quad (1)$$

where  $\sigma_{max}$  is the maximum stress acting at the notch tip and  $\sigma_n$  is the nominal stresses that would act there if the notch had no effect on the stress field that surrounds it.

Like all LE parameters,  $K_t$  are unique values that can be cataloged and then used to solve many important notch problems in structural engineering. They are particularly useful for designing against fatigue crack initiation, for example. However, to properly describe notch effects in elastoplastic analyses, or in multiaxial loading problems, or in anisotropic materials, or even to consider 3D effects in simple uniaxial LE cases (e.g. when the notch tip radius is in the order of or smaller than the component thickness), it is necessary to separate stress from strain concentration effects. In such cases, different stress and strain concentration factors may be defined by  $K_\sigma = \sigma_{max} / \sigma_n$  and  $K_\epsilon = \epsilon_{max} / \epsilon_n$ , respectively, as discussed elsewhere [1,2].

Pioneer analytical solutions for LE SCF were obtained by Kirsch in 1898 [3], who studied the effect of a circular hole in a tensioned infinite plate, and by Inglis in 1913 [4], who solved the similar

<sup>\*</sup> Corresponding author.

E-mail addresses: [jtcastro@puc-rio.br](mailto:jtcastro@puc-rio.br) (J.T.P. Castro), [dsimoes3@gmail.com](mailto:dsimoes3@gmail.com) (D. Simões), [ivan@puc-rio.br](mailto:ivan@puc-rio.br) (I.F.M. Menezes), [meggi@puc-rio.br](mailto:meggi@puc-rio.br) (M.A. Meggiolaro), [lfm@tecgraf.puc-rio.br](mailto:lfm@tecgraf.puc-rio.br) (L.F. Martha).

elliptical hole problem. Since then, a few analytical and many other numerical and experimental  $K_t$  values have been obtained for countless notch geometries. However, most of them by modeling the notches as if they could be properly described by a 2D approximation, solving the stress analysis problem assuming LE plane stress ( $pl-\sigma$ ) or eventually plane strain ( $pl-\varepsilon$ ) conditions around their tips. Peterson is a traditional SCF catalog [5], although mostly restricted to plane and axisymmetric LE solutions, whereas Savin [6] is a classical reference for analytical SCF solutions.

A traditional procedure to decrease  $K_t$ -effects is to round notch tips using as large as possible circular arcs. This design rule is clearly justified by the classic Inglis' solution for elliptical notches [4], which in the simplest uniaxial case leads to

$$K_t = 1 + 2a/b = 1 + 2\sqrt{a/\rho} \quad (2)$$

where  $a$  and  $b$  are the semi-axes of the elliptical hole in an infinite plate loaded by a normal nominal stress perpendicular to  $a$ , and  $\rho = b^2/a$  is its smallest radius, which occur at the extreme of its  $2a$  axis, so at the points that can be called the elliptical notch tips.

However, although outside the scope of this work, it is important to emphasize that  $K_t$  values are not sufficient to quantify all notch-induced stress concentration effects. In fact, both the maximum stresses at the notch tips and the stress gradients around them can significantly affect the actual resistances and consequently the operational lives of structural components. The stress gradient is the main responsible for notch sensitivity under fatigue and under EAC conditions, so very sharp notches are not as bad as it could be anticipated from their very high  $K_t$  values because they have very sharp gradients as well, as discussed elsewhere [7,8]. Anyway, to decrease deleterious effects that can be introduced by sharp notches in structural components, their tips are usually rounded or blunted by circular arcs. The larger such tips radii are the better, meaning the more they tend to alleviate all stress concentration effects induced by the notches. Such facts are well known, and all structural engineers and wise technicians specify generous rounding radii for their notch tips.

Less well known is the fact that circular arcs decrease but do not minimize stress concentration effects around notch tips. Even though this problem has been recognized for a long time, notches with variable radius tips properly optimized to minimize their detrimental influence on the strength of structural components still are not as widely used in engineering designs as they should be. Indeed, albeit efficient receipts for improving notch profiles have been proposed in the early 1930s, the usual practice still is to specify notches with as large as possible constant radius tips, probably because they can be easily fabricated in traditional manually-operated machine tools. To enhance this argument, it can be pointed out that not even standard fatigue crack initiation test specimens are specified with optimized notches to connect their uniform test section to the larger heads required to grip them [9–12]. Indeed, the generous constant radius notch tips used to significantly alleviate their stress concentration effects do not minimize them. Since such notches locally concentrate stresses and strains around their roots, they may localize the crack initiation point, invalidating in this way the test results, or at least increasing their already intrinsically high dispersion.

On the other hand, natural structural members such as tree branches and bones have learned by evolution to add material where it is needed, so their notches have variable instead of the fixed radii usually specified to smooth engineering notch tips [13–17]. Since notches with properly specified variable tip radius can have much lower SCF than those obtainable by fixed notch root radii of similar size, such improved notches can be a very good design option to increase fatigue strengths with almost no side effects on the global dimensions or on the weight of most structural components. Moreover, properly optimized notches are

now more useful than ever, as nowadays they can be economically specified and manufactured due to the widespread availability of finite elements (FE) codes to calculate and of computer controlled machine tools to fabricate them. These smart design practices can be much cheaper and wiser substitutes for expensive high-performance materials or for major reinforcements in components that tend to fail under service loads.

The aim of this note is first to compare the efficiency of both traditional and modern receipts to design better notch tip profiles, and then to analyze the SCF improvements achievable by optimizing the variable tip radii of notches for uniaxial and multiaxial load applications, using the FE method. To optimize the notches, a simple gradientless optimization method, based on the idea of iteratively adding material where it is needed and removing it where it is superfluous, is proposed and implemented using a self-adaptive remeshing scheme that can be easily adapted to be compatible with most commercial finite element (FE) codes. This technique is used to improve the notches of push–pull, rotary bending, alternated bending, and multiaxial tension–torsion fatigue test specimens, as well as the shape of a tension–torsion load cell, but it can be equally used to optimize any other notch problem. Finally, a more powerful notch-tip optimization method that also considers gradient effects around them is described and evaluated.

## 2. Notch improvement fundamentals

Peterson [5] says that notches tips with variable radii have long been intuitively used on old cast components, and lists some early works in this area that can still be used as very good design practices. He mentions for instance Baud's fillet for tension loads proposed in 1934, based on the shape of the laminar stream of an ideal frictionless liquid flowing by gravity from a large tank with a hole at the bottom, as shown in Fig. 1(left). The analytical solution for this problem generates a transition region whose coordinates are given by:

$$x = (2d/\pi) \cdot \sin^2(\theta/2) \text{ and } y = 2 \cdot \log[\tan(\theta/2 + \pi/4) - \sin \theta] \quad (3)$$

To improve the fatigue strength of shafts, Thum and Bautz's proposed also in 1934 an improved notch shape for bending and torsion loads, which they claimed could even eliminate the notch deleterious effect on fatigue lives, as also mentioned in [5]. The proportions of these two improved fillet shapes are listed in Table 1, and the listed values are used in Fig. 1(right) to plot their actual shapes in scale. Moreover, if  $y$  is the coordinate along the shaft axis,  $d_f$  is its diameter along the fillet profile, and  $d$  is its smallest diameter, Baud's and Thum and Bautz's improved fillets can be fitted within less than 0.12% rms error by Eqs. (4) and (5), which can be easily programmed e.g. in CNC lathes:

$$\frac{d_f}{d} = 1 + \frac{(y/d)^2 - 4 \cdot y/d + 3.7}{29 \cdot y/d + 6} \text{ if } y/d < 1.45, \text{ otherwise } d_f \cong d \text{ (for tension)} \quad (4)$$

$$\frac{d_f}{d} = 1 + \frac{y/d + 0.0068}{68(y/d)^3 + 33(y/d)^2 + 3.3y/d + 0.014}, \text{ if } y/d \geq 0 \text{ (for bending or torsion)} \quad (5)$$

Peterson mentions as well two other old ideas for improving notch profiles: 15–20° tapered fillets with smoothed ends for shaft shoulders proposed by Morgenbrod in 1939, and Grodzinski's graphical recipe for shoulder fillets proposed in 1941, which divides the shoulder space in equally spaced intervals, and then orderly joins them by straight lines, as sketched in Fig. 2. These intervals should be larger in the smaller side of the shoulder section, as illustrated in the figure, and the final notch shape should be smoothed to remove the kinks between the line segments.

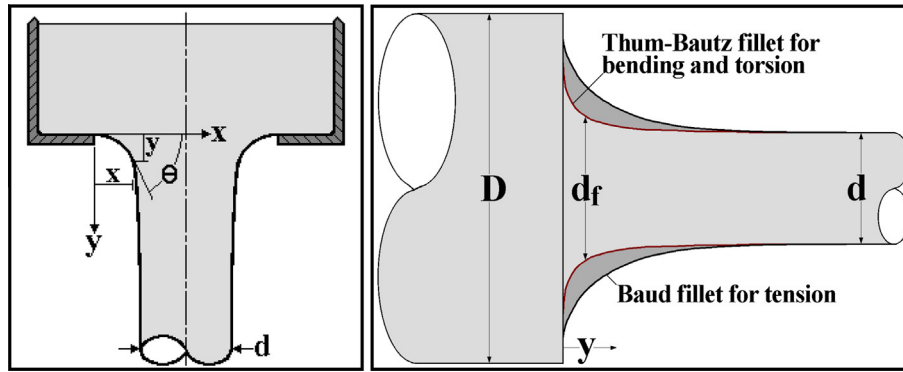


Fig. 1. (left) Baud's fillet for tension loads based on a hydrodynamic analogy; (right) Baud's and Thum-Bautz's variable radius shoulder fillets to minimize  $K_t$  effects for tension and for bending or torsion loads, drawn in scale from Table 1 points.

Table 1  
Improved fillets for round bars loaded in tension, torsion (T), or bending (B).

|                       |       |       |       |       |       |       |       |       |       |       |          |
|-----------------------|-------|-------|-------|-------|-------|-------|-------|-------|-------|-------|----------|
| $y/d$                 | 0.000 | 0.002 | 0.005 | 0.010 | 0.020 | 0.040 | 0.060 | 0.080 | 0.100 | 0.150 | 0.200    |
| $d_f/d$ for tension   | 1.636 | 1.610 | 1.594 | 1.572 | 1.537 | 1.483 | 1.440 | 1.405 | 1.374 | 1.310 | 1.260    |
| $d_{fT}/d$ for T or B | 1.475 | 1.420 | 1.377 | 1.336 | 1.287 | 1.230 | 1.193 | 1.166 | 1.145 | 1.107 | 1.082    |
| $y/d$                 | 0.300 | 0.400 | 0.500 | 0.600 | 0.700 | 0.800 | 0.900 | 1.000 | 1.300 | 1.600 | $\infty$ |
| $d_f/d$ for tension   | 1.187 | 1.134 | 1.096 | 1.070 | 1.051 | 1.037 | 1.027 | 1.019 | 1.007 | 1.004 | 1.000    |
| $d_{fT}/d$ for T or B | 1.052 | 1.035 | 1.026 | 1.021 | 1.018 | 1.015 | 1.012 | 1.010 | 1.005 | 1.003 | 1.000    |

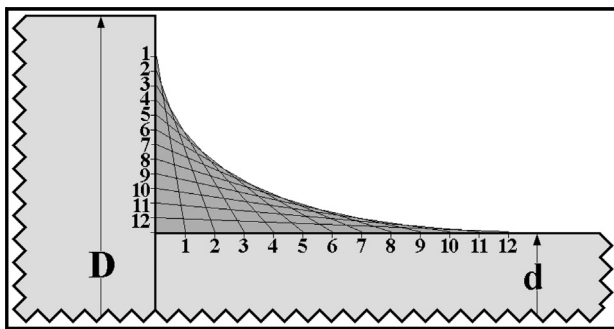


Fig. 2. Grodzinski's variable radius improved shoulder fillets, generated by first dividing their limits in the same number of equally spaced intervals, with larger intervals in the smaller diameter side, and then by orderly joining them by straight lines.

Unlike usual engineering components, natural structural members like tree branches and bones typically grow with variable radii notches to minimize the unavoidable stress concentration effects associated with their connections, as illustrated in Fig. 3. Heywood [14] and Mattheck [15,16] study the natural SCF reduction processes in deeper detail. Mattheck and Burkhardt proposed [17] in 1990 a simple procedure for improving notch shapes based on the apparent self-growth mechanism of tree branches. Realizing that force lines are bent by the notches, they assume stress concentration effects are due to the superposition of local bending stresses on the tensile stresses that would act there. Thus, they assume their SCF can be decreased by shaping their contour to substitute bent force lines around their borders by stretched ones, the main idea behind the “method of tensile triangles” for improving the notch geometry, as schematized in Fig. 4.

So, according to Mattheck, sharp corner-like notches can be reinforced by a tensile triangle to reduce its local stresses, creating two new notches with less dangerous larger angles, and be further streamlined starting with a 45° rectangular triangle and them successively adding obtuse isosceles triangles to reinforce the weaker notch side, as shown in Fig. 4. The second triangle departs from the

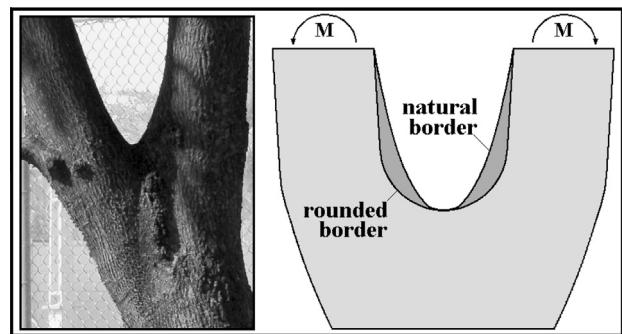


Fig. 3. Natural notches usually do not have a constant radius tip, as nature knows better how to minimize stress concentration by adding material where it is needed.

middle of the first one, the third from the middle of the second, and so on. The more triangles, the smaller is the  $K_t$  of the improved notch. After smoothing the kinks between the reinforcing triangles, this simple graphical construction generates a near optimum notch contour, a claim verified by FE analyses, see Fig. 5 [16]. Moreover, this notch shape can be scaled to fit space limitations, since it is dimension-independent. Tensile triangles can also be used to remove unloaded material in un-notched regions, saving weight without compromising the structure strength.

An even simpler improved shape for shoulder fillet tips is to use one eighth instead of one quart of a circular arc to round them, starting their 45° junction at the larger side of the shoulder. Tensile triangles and 1/8 circular arcs are particularly useful in practice, since they can be easily built in CNC machine tools. Lacking better information, these simple receipts probably can also be used to improve notch shapes designed for multi-axial loading conditions. However, for non-symmetric loads, the improved notch tip profile should not be symmetric. Instead it should be properly adjusted according to the load ratio, so that the deepest notch point should be shifted towards the less loaded substructure as illustrated in Fig. 6, which is schematically drawn based on the method of tensile triangles. Natural structures follow this rule, and the deepest

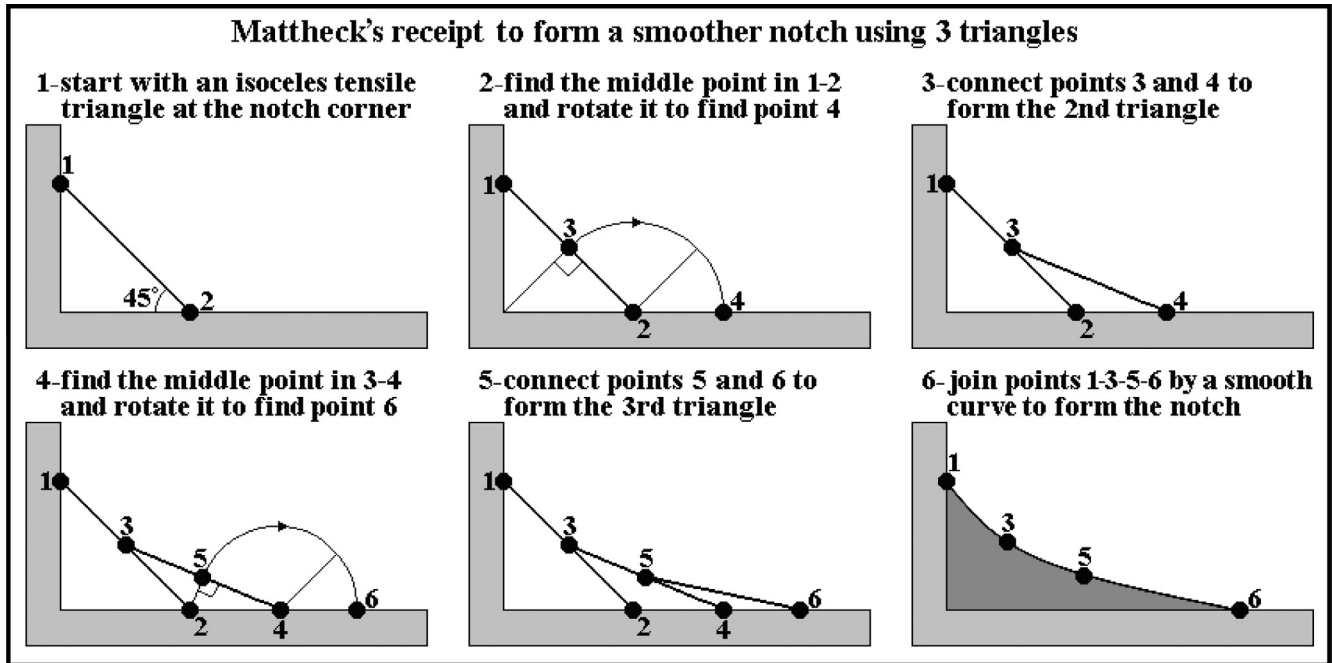


Fig. 4. Mattheck's tensile triangle method to improve notch profiles.

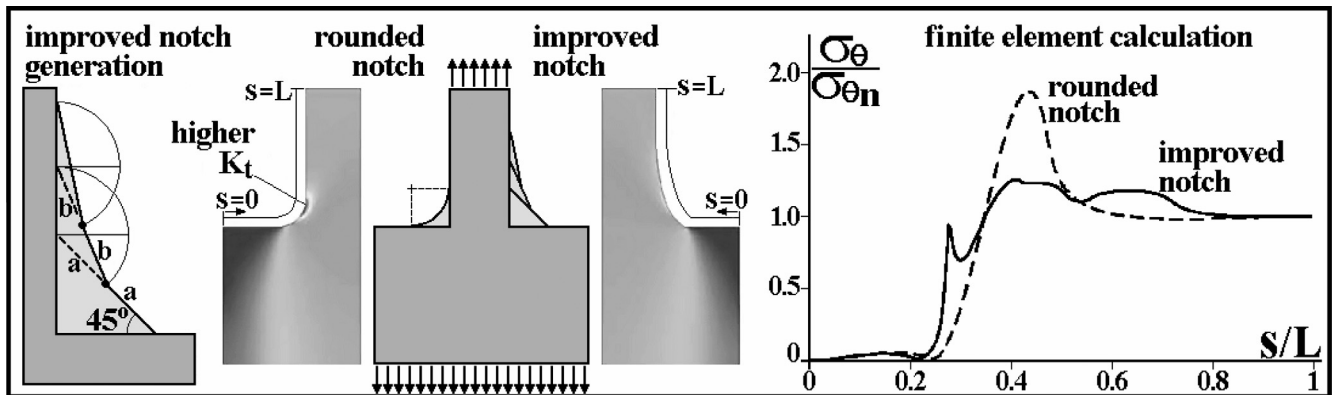


Fig. 5. Improved shoulder with 3 tensile triangles at a corner side, starting from a 45° rectangular triangle; photoelastic fringes of a quart-circular and of such an improved notch; and FE results quantifying its efficiency (adapted from [15]).

points of their notches indicate for which load ratio they have been designed for (or rather evolved to).

Fig. 7 shows the stress concentration effects induced on the stress distribution along a shoulder fillet on a flat bar pulled by a centered tensile load, calculated by a refined FE analysis, for the improved variable tip radii fillets proposed by Mattheck, Grodzinski, and Baud, and also for the traditional 1/4 of a circle tip used for comparison purposes. In view of their efficacy to reduce stress concentration effects, it is quite surprising to see such variable radii improved fillets neglected by many modern designers. Indeed, if correctly applied, they can considerably decrease the  $K_t$  values and, consequently, increase the fatigue lives of structural components at a very attractive cost.

### 3. Basic shape optimization procedures to reduce stress concentration effects

Lansard points out in his 1954 work that improved progressive curvature fillets with near constant stresses along their tip profile can even reduce their  $K_t$  to unit if their tips are large enough,

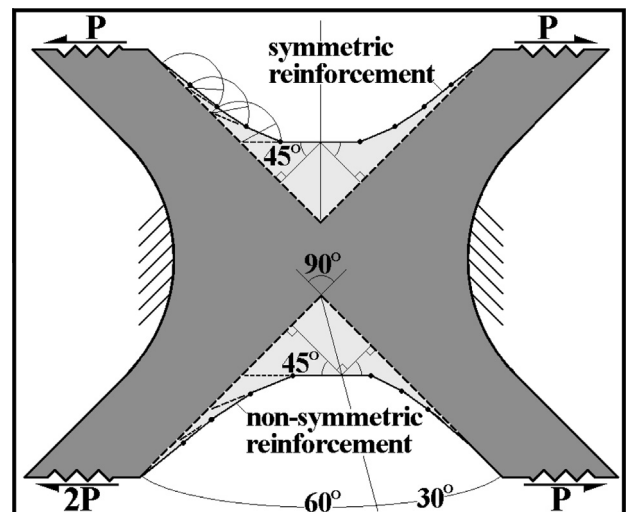


Fig. 6. Symmetrical loads require symmetrical notches, but asymmetrical loads need asymmetrical notches, with more material added to their most loaded branches.

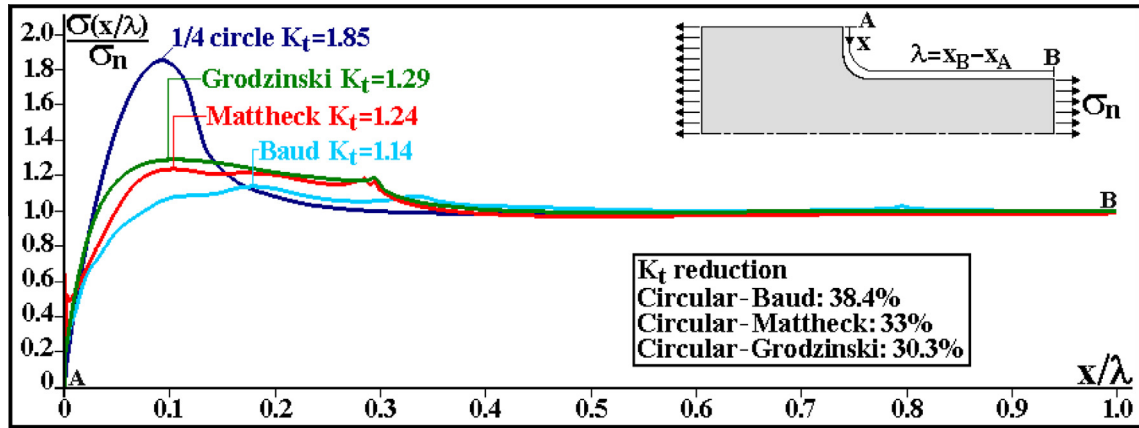


Fig. 7. The stress distribution along improved variable radius fillets illustrates well the advantages of using such notch shapes instead of the traditional 1/4 of a circle shoulder.

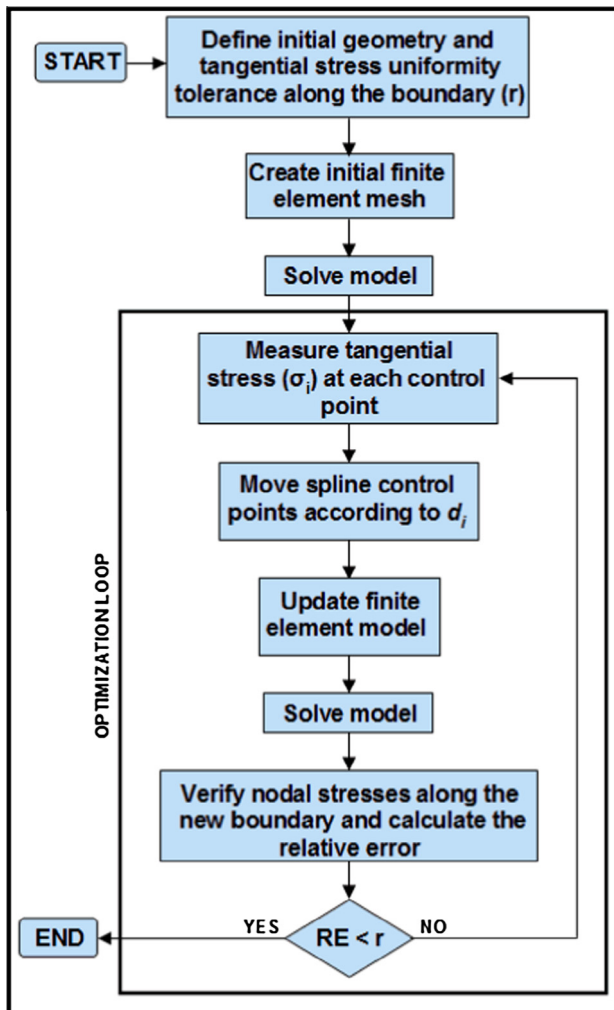


Fig. 8. Flowchart of the spline-based gradientless optimization method.

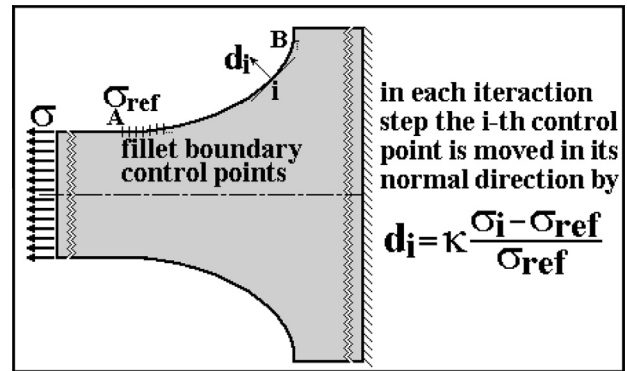


Fig. 9. Simple gradientless optimization method to improve the fillet shape in a flat bar subjected to a remotely uniform tensile loading.

eliminating in this way their detrimental stress concentration effects. This claim indicates that optimum notch tip profiles should be designed to maintain the stresses as fixed as possible along them [13], adding material where it is needed and removing it where the stresses are too low, simulating in this way the ideal natural growth behavior.

Many studies on notch shape optimization algorithms based on different approaches confirm this claim. For example, Sonmez based his optimization process on a stochastic algorithm called the direct search simulated annealing, which relies on a thermodynamic analogy to search for the lowest energy state, looking for a fillet tip boundary shape that results in a minimum tangential stress [18–20]. Das et al. used evolutionary structural optimization (ESO) algorithms that slowly remove unloaded material to arrive at the optimum notch tip shape [21]. A photoelastic model of a notch shape optimized by Schnack from an initially semicircular root shown in Ref. [22] is a particularly interesting visual proof that illustrates well how this process can indeed induce an almost uniform tangential stress distribution along the notch boundary. Finally, Meneghetti et al. [23] have recently extended the peak stress method (PSM) for fatigue design of welded joints considering complex 3D FE models. According to the authors, this method is based on the property that the ratio between the mode I notch intensity factor and the linear elastic opening peak stress, evaluated at the crack tip by the FE method (as well as the ratio between the mode II stress intensity factor and the sliding peak stress), depends only on the type and on the size of the elements adopted in the discretization. Therefore, the PSM method can be combined with 3D FE models to become an efficient computational tool to assess the fatigue strength of joints with complex geometries.

### 3.1. Gradientless strategies

Among the many optimization strategies, the gradientless algorithm is a particularly interesting numerical technique for

minimizing SCFs. Its idea is simple and intuitive: it iteratively adds material where the stresses are higher than desired, and removes it where the stresses are too low, looking for as uniform as possible tangential or Mises stresses along the entire notch tip profile [24–27]. Moreover, since the gradientless strategy does not use stress derivatives, it simplifies the shape optimization process because its numerical implementation is intrinsically robust. Indeed, in the simple algorithm developed for this work, the notch boundary is modeled by cubic splines, defined by control points distributed along its profile. The optimal tip shape is achieved iteratively by moving such control points to simulate how notches grow in natural structures by using material where it is really needed, as depicted in the gradientless algorithm flow chart presented in Fig. 8.

For example, Fig. 9 shows a notched flat bar loaded under pure tension, with an initially variable stress distribution along its shoulder fillet profile. This spline-based gradientless optimization method seeks for a constant tangential stress along the notch boundary, changing its shape by moving its control points according to the simple equation presented in the figure. The movement

$d_i$  of each control depends on its tangential stress  $\sigma_i$ , and on a reference stress  $\sigma_{ref}$  at point A, which is fixed. A factor  $\kappa$  may be used to accelerate this iterative optimization process, which repeatedly calculates the stress at each control point in a finite element (FE) environment and compares it with the desired reference stress. If it is lower, material is removed from that point (by moving it by a negative small step  $d_i$ ); if it is higher, material is added to it.

3.2. Gradient strategies

On the other hand, several optimization methods, based on sensitivity analysis, for minimizing the stress concentration along a design boundary have been presented in the literature [28–30]. Although the computation of gradients (i.e. stress derivatives) may be an expensive task for problems with large number of variables, the overall computational cost is usually reduced when gradient information is introduced into the optimization process.

The computational efficiency of optimization algorithms used for finding optimal boundary shapes is highly dependent on the representation of the boundary. Hence, geometric modeling plays

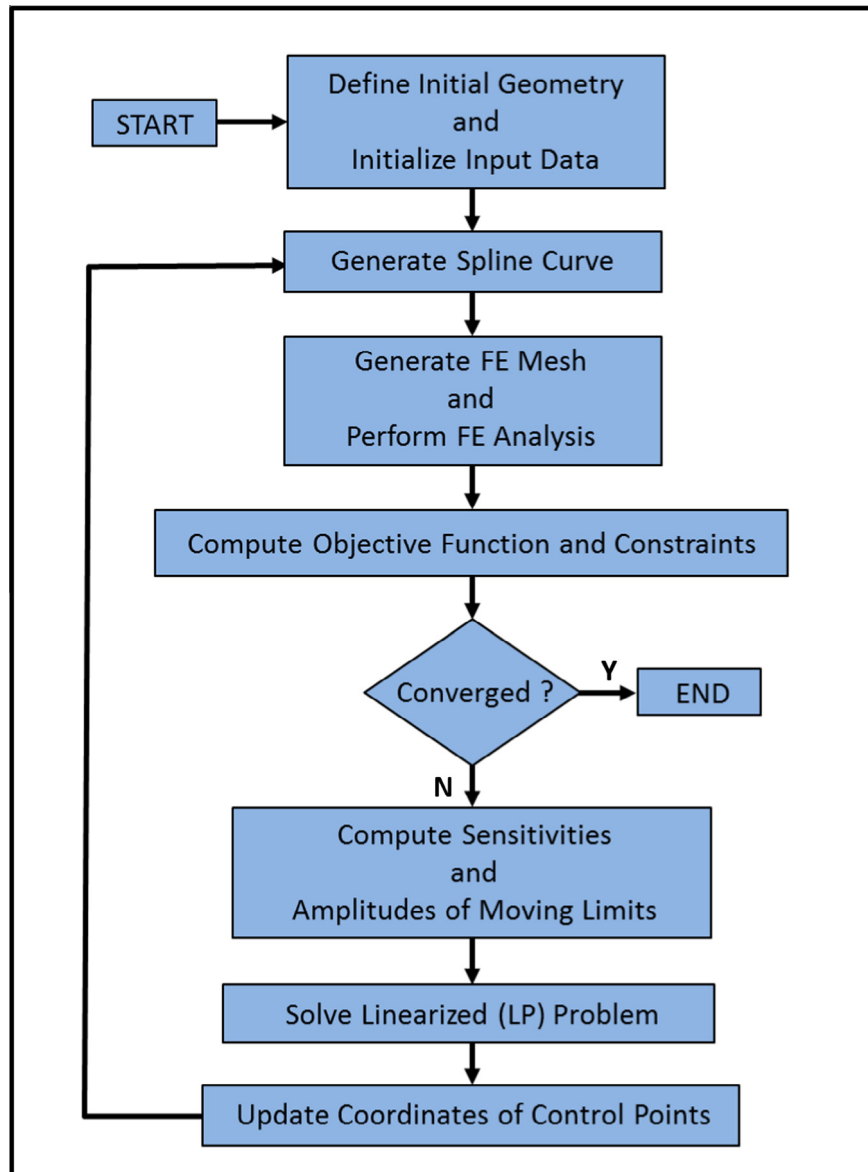


Fig. 10. Flowchart of the spline-based gradient optimization method.

an important role in shape optimization processes. SCF minimization problems are in particular highly sensitive to the choice of appropriate design variables to model the notch tip boundary curve. Many researchers define the coordinates of the boundary nodes in the FE mesh as the design variables [24,25]. Depending on the level of mesh refinement, this approach may require a large number of design variables and constraints, increasing in this way the computational cost. Moreover, it is necessary to smooth the nodal movements since nodal stresses are very sensitive to the position of neighboring boundary nodes, especially for refined meshes.

To overcome this problem in practice, well-known methods for geometric representation of the design boundary, based on parametric splines curves, are often used. For instance, a reduced number of control points (when compared to the number of boundary nodes) is distributed along the boundary profile [27]. The optimal shape is achieved by moving such control points according to each step of the optimization algorithm, as illustrated in the flow chart depicted in Fig. 10. In this work we propose a gradient-based shape optimization method for minimizing SCF defined as:

$$\begin{cases} \text{Min } f(\mathbf{x}), & \mathbf{x} \in \mathbb{R}^n \\ \text{Subjected to: } & g_j(\mathbf{x}) \leq 0, \quad j = 1, \dots, m \\ & x_i^L \leq x_i \leq x_i^U, \quad i = 1, \dots, n \end{cases} \quad (6)$$

where  $f(\mathbf{x})$  is the objective function,  $\mathbf{x}$  is the vector of  $n$  design variables,  $g_j(\mathbf{x})$  is the  $j$ -th inequality constraint,  $x_i^L$  and  $x_i^U$  are the box constraints, and  $m$  is the number of inequality constraints. The objective function is defined as the least-squares function given by:

$$f(\mathbf{x}) = \sum [\sigma_i(\mathbf{x}) - \sigma_{ref}]^2, \quad i = 1, \dots, n \quad (7)$$

where  $\sigma_i$  is the tangential stress (or the Mises stress) at the  $i$ -th spline control point and  $\sigma_{ref}$  is a reference stress value. The design variables are the coordinates of each spline control point. As pointed out by Carbonari et al. [30], since the optimization algorithm moves each point in the normal direction to the spline curve, only  $\mathbf{x}$  (or  $\mathbf{y}$ ) coordinates are chosen, which reduces the size of the optimization problem.

Fig. 11 shows a notched flat bar loaded under pure tension, with an initially variable stress distribution along its shoulder fillet profile. The proposed spline-based gradient optimization method is an

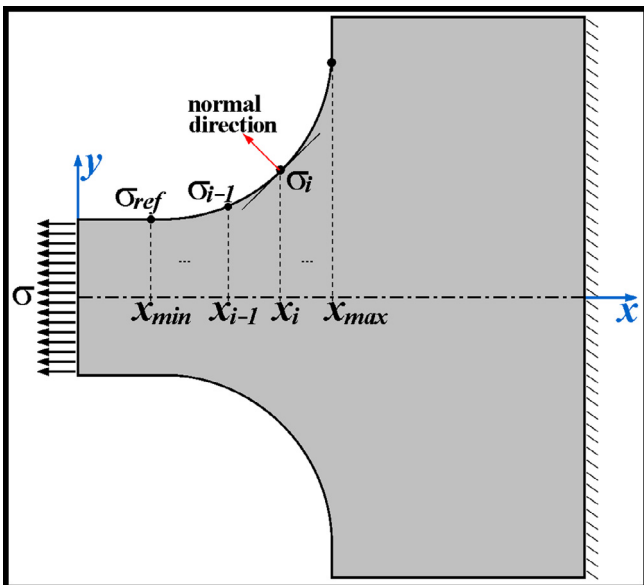


Fig. 11. Gradient-based optimization method to improve the fillet shape in a flat bar subjected to a remotely uniform tensile loading.

iterative process that aims to minimize the stress distribution along the notch boundary by changing the position of the spline control points until the stress distribution is constant (or near constant), within a prescribed numerical tolerance. For each step of the optimization algorithm a FE analysis is performed and the stresses are evaluated at each control point. The stresses, as well as their derivatives with respect to the design variables, are then used by the optimization algorithm to define the new shape of the design boundary. To avoid numerical oscillations during the shape optimization process, Carbonari et al. [30] suggest the introduction of some constraints:

$$\begin{cases} x_1 \geq x_{min} \\ x_i - x_{j-1} \geq \varepsilon, \quad j = 2, \dots, n - 1 \\ x_n \leq x_{max} \end{cases} \quad (8)$$

where  $\varepsilon$  is a given small number,  $\mathbf{x}$  are the design variables, and  $x_{min}$  and  $x_{max}$  are the prescribed lower and upper bounds for the design variables, respectively, as illustrated in Fig. 11.

The sensitivity of the objective function, with respect to the design variables, is obtained numerically by means of the finite difference method, i.e.:

$$\partial f(\mathbf{x}) / \partial x_i = [f(x_1, x_2, \dots, x_i + \nabla x, \dots, x_n) - f(\mathbf{x})] / \nabla x \quad (9)$$

where  $\nabla x$  is a numerical perturbation usually taken as a small percentage of the initial spline length (e.g.  $\nabla x = 0.01 L_s$ , where  $L_s$  is the approximated spline length) [30].

This optimization problem is solved here using the well-known Sequential Linear Programming (SLP) algorithm [31]. To obtain feasible solutions in each optimization process step, and also to prevent the linear approximations to the problem to become unbounded, especially for under-constrained problems, a moving limit strategy is usually required by the SLP algorithm. It consists of defining box constraints for each design variable. The amplitude of the moving limits ( $\delta$ ) is also defined here as a fraction of the initial spline length (e.g.,  $\delta = 0.2 L_s$ ) and is usually decreased as the solution of the approximated linear problem is achieved at each step. Finally, the complete gradient-based shape optimization problem proposed here can be expressed in a standard form as:

$$\begin{cases} \text{Min} & f(\mathbf{x}) = \sum [\sigma_i(\mathbf{x}) - \sigma_{ref}]^2, \quad i = 1, \dots, n \\ \text{subjected to:} & -x_1 + x_{min} \leq 0 \\ & x_{j-1} - x_j + \varepsilon \leq 0, \quad j = 2, \dots, n - 1 \\ & x_n - x_{max} \leq 0 \\ & x_i^L \leq x_i \leq x_i^U, \quad i = 1, \dots, n \end{cases} \quad (10)$$

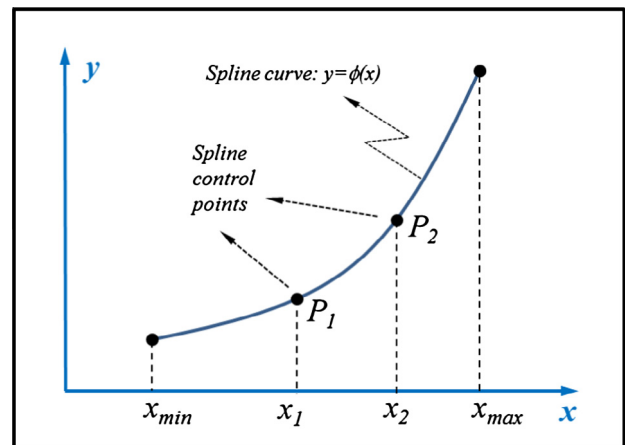


Fig. 12. Spline control points and corresponding boundary curve.

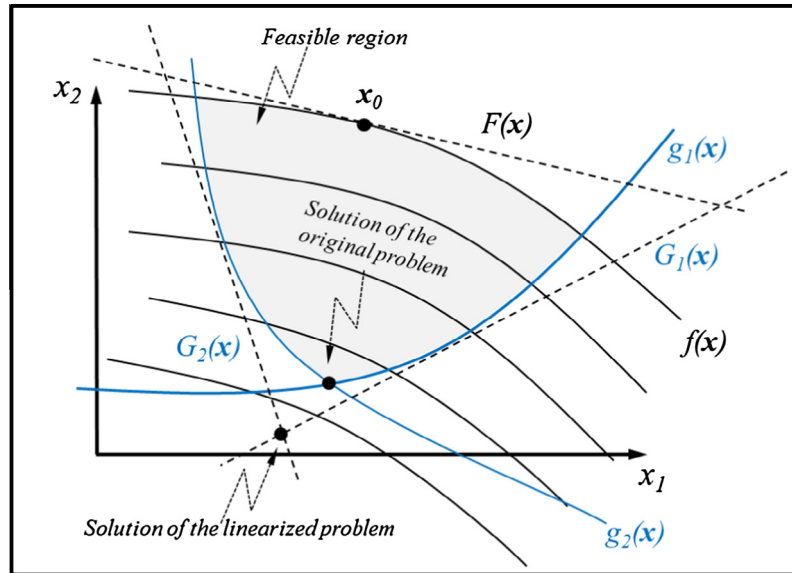


Fig. 13. Graphical interpretation of the linearized optimization problem (adapted from [31]).

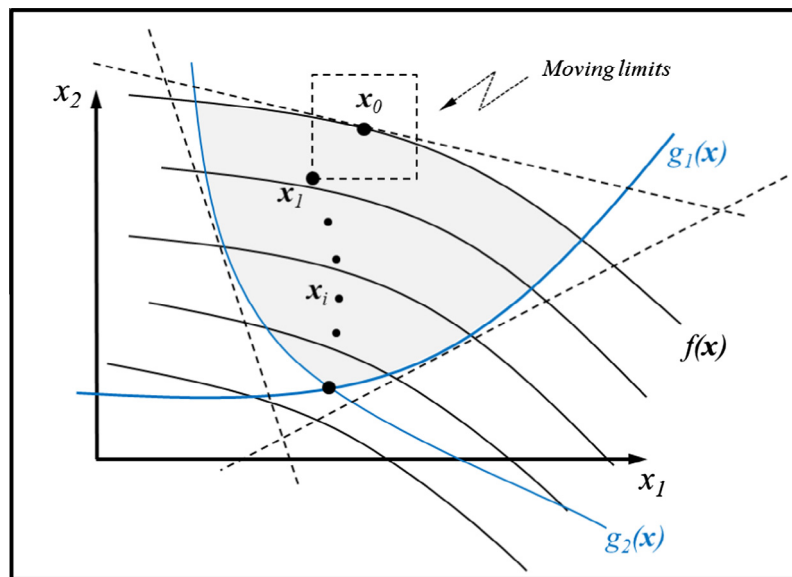


Fig. 14. Moving limits and sequence of the linearized solutions (adapted from [31]).

To better understand the main steps of the proposed SLP gradient-based algorithm, consider a simplified version of the problem shown in Fig. 11, where only two design variables ( $x_1, x_2$ ) are used to represent the boundary shape, as illustrated in Fig. 12. For a given set of design variables a spline curve (usually defined as a smooth polynomial piece-wise function)  $y = \phi(x)$  is used to describe the boundary shape.

Let  $\mathbf{x}_0$  be an initial guess for the design variables (i.e., initial position of the control points). The first step of the SLP algorithm consists of linearizing the objective and constraint functions of the original optimization problem by means of the first-order Taylor series expansions. Eq. (6) can be rewritten as:

$$\begin{cases} \text{Min} & F(\mathbf{x}) \cong f(\mathbf{x}_0) + \nabla f(\mathbf{x}_0) \cdot (\mathbf{x} - \mathbf{x}_0) \\ \text{Subjected to:} & G_j(\mathbf{x}) \cong g_j(\mathbf{x}_0) + \nabla g_j(\mathbf{x}_0) \cdot (\mathbf{x} - \mathbf{x}_0) \leq 0, \quad j = 1, \dots, m \\ & x_i^l \leq x_i + (x_i - x_{0i}) \leq x_i^u \quad i = 1, \dots, n \end{cases} \quad (11)$$

where  $F(\mathbf{x})$  and  $G_j(\mathbf{x})$  are the linear approximations about  $\mathbf{x}_0$  of functions  $f(\mathbf{x})$  and  $g_j(\mathbf{x})$ , respectively, and “ $\cdot$ ” is a dot product notation.

Eq. (11) now represent a linear programming problem which can be solved by any algorithm, for example: Simplex or Interior Point Methods [31,32]. Fig. 13 shows a graphical interpretation of the linearized solution for the two variable optimization problem proposed in Fig. 12. As mentioned before, in order to prevent the linearized solution to be unfeasible (or unbounded in some situations) moving limits (or box constraints) are introduced in the linear approximation, as illustrated in Fig. 14. Finally, during the optimization process the amplitudes of the moving limits are reduced such that the approximated solution can be obtained as close as possible to the solution of the original problem. Each approximated solution ( $\mathbf{x}_0, \mathbf{x}_1, \dots, \mathbf{x}_i, \dots$ ) corresponds to a different spline curve (boundary shape) until convergence is achieved.

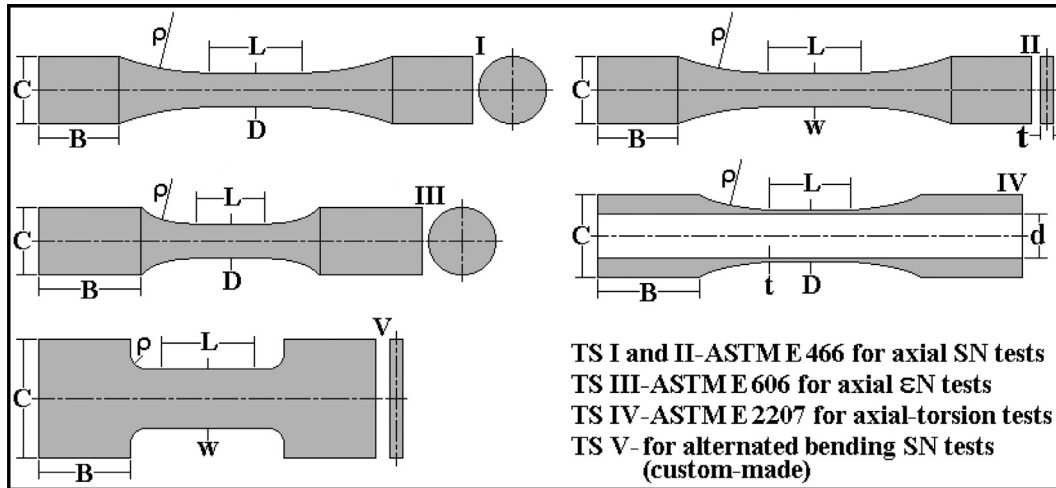


Fig. 15. Fatigue test specimens.

Table 2  
Dimensions of the studied fatigue TS (see ASTM standards for details).

| TS dimensions (in mm) |                                     | I     | II    | III   | IV   | V     |
|-----------------------|-------------------------------------|-------|-------|-------|------|-------|
| <i>L</i>              | Length of the straight test section | 76.2  | 63.5  | 19.05 | 42   | 10.16 |
| $\rho$                | Original (circular) notch radius    | 203.2 | 203.2 | 50.8  | 89.6 | 3.18  |
| <i>D</i>              | Circular test section diameter      | 25.4  | -     | 6.35  | 28   | -     |
| <i>w</i>              | Rectangular test section width      | -     | 25.4  | -     | -    | 6.35  |
| <i>C</i>              | Gripping head diameter/width        | 50.8  | n/a   | 12.7  | 44.8 | 12.7  |
| <i>B</i>              | Gripping head length                | 60    | 60    | 19.05 | 56   | 10    |
| <i>d</i>              | Inner diameter (of the tubular TS)  | -     | -     | -     | 24   | -     |
| <i>t</i>              | Thickness                           | -     | n/a   | -     | 2    | -     |

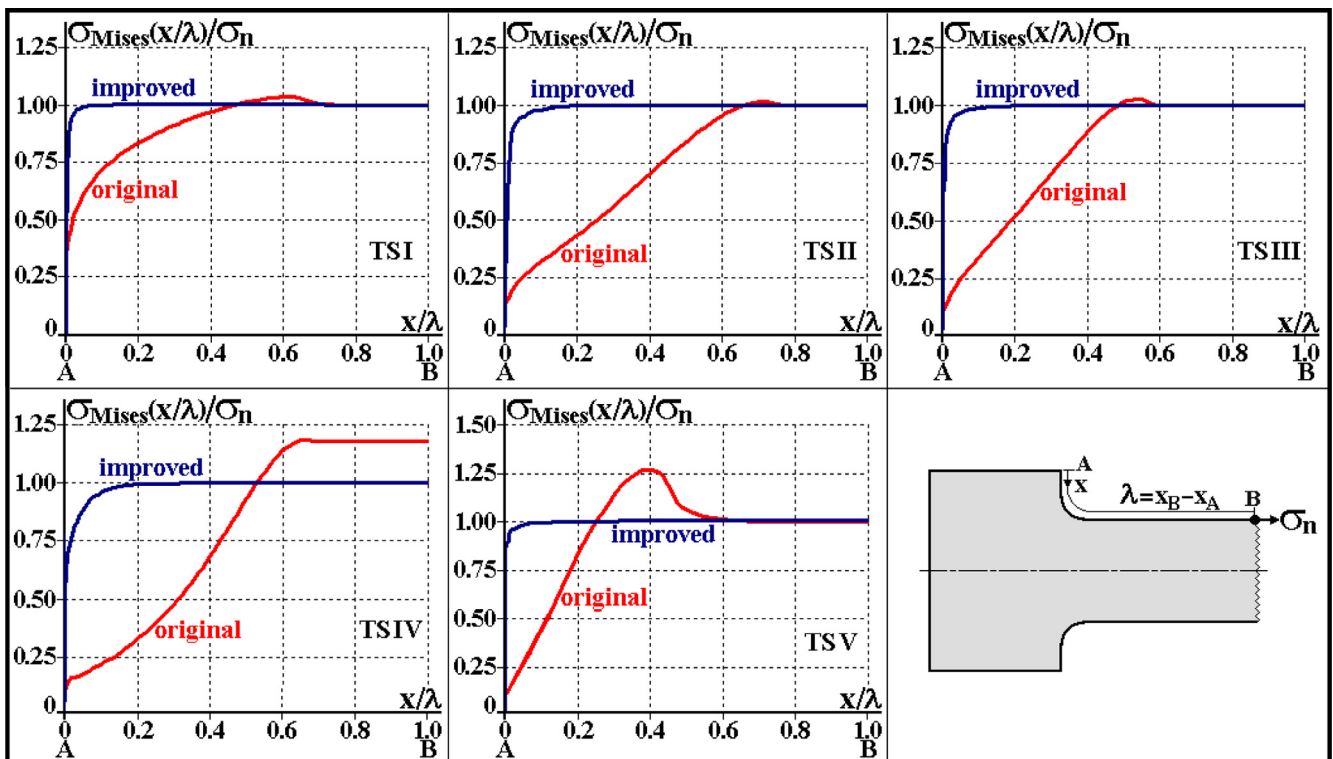


Fig. 16. Mises stress along the original and the improved fillets boundaries.

#### 4. Optimized fatigue test specimens

As mentioned before, some standard fatigue testing specimens (TSs) do not have optimized notch shapes. Most of them have quite low SCFs, but which can be decreased by improving their notch profiles. Moreover, some have surprisingly high  $K_t$ , which should be improved. So, a good illustration of the spline-based gradient-less optimization method usefulness for generating better notch profiles in practical applications is to use it to reduce even more

the SCF of standard push–pull and rotating bending fatigue test specimens, and also to improve the standard tension–torsion TS, as well as a custom-made alternated bending TS especially designed for making fatigue crack initiation tests in relatively thin sheets of a high strength steel, see Fig. 15 and Table 2.

Types I–IV are traditional ASTM TSs [9–12], whereas TS type V is an unconventional flat specimen designed to be used in an especial four-point alternated bending fixture. All such fatigue TSs use an irregular circular arc notch tip profile to connect their uniform test

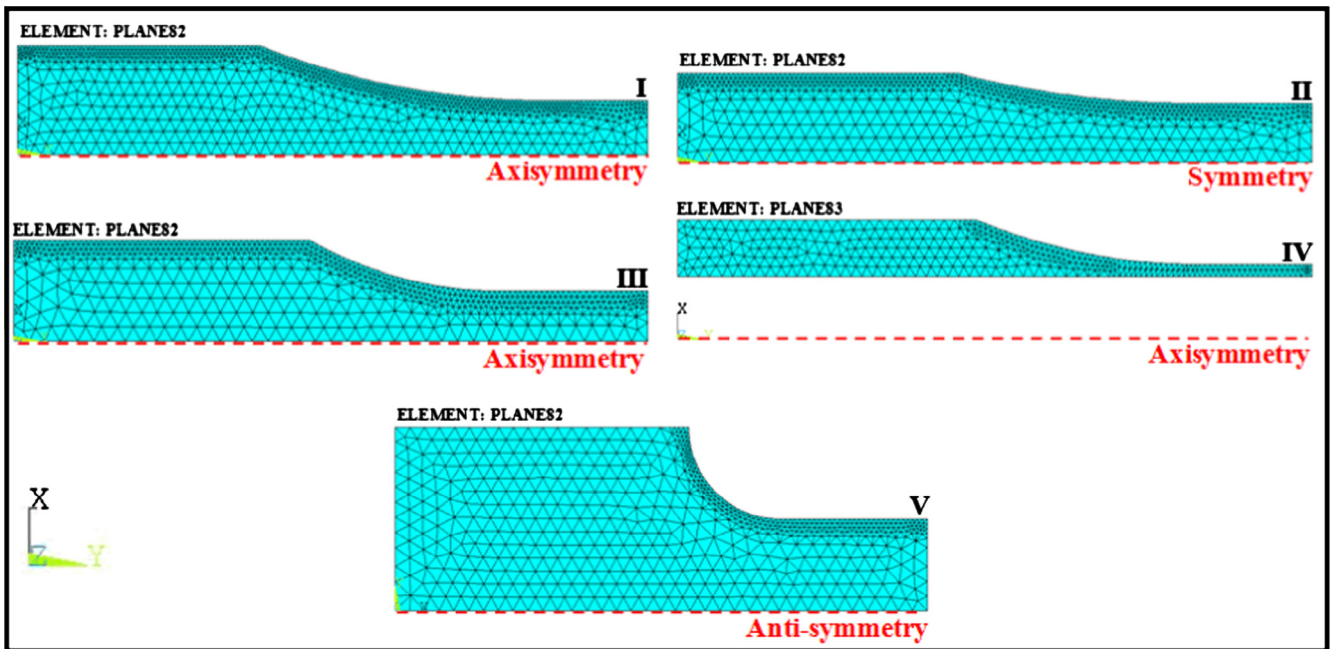


Fig. 17. Final finite element meshes generated by the spline-based gradient optimization method for type I–IV standard ASTM fatigue test specimens and for type V custom made alternated bending fatigue specimen.

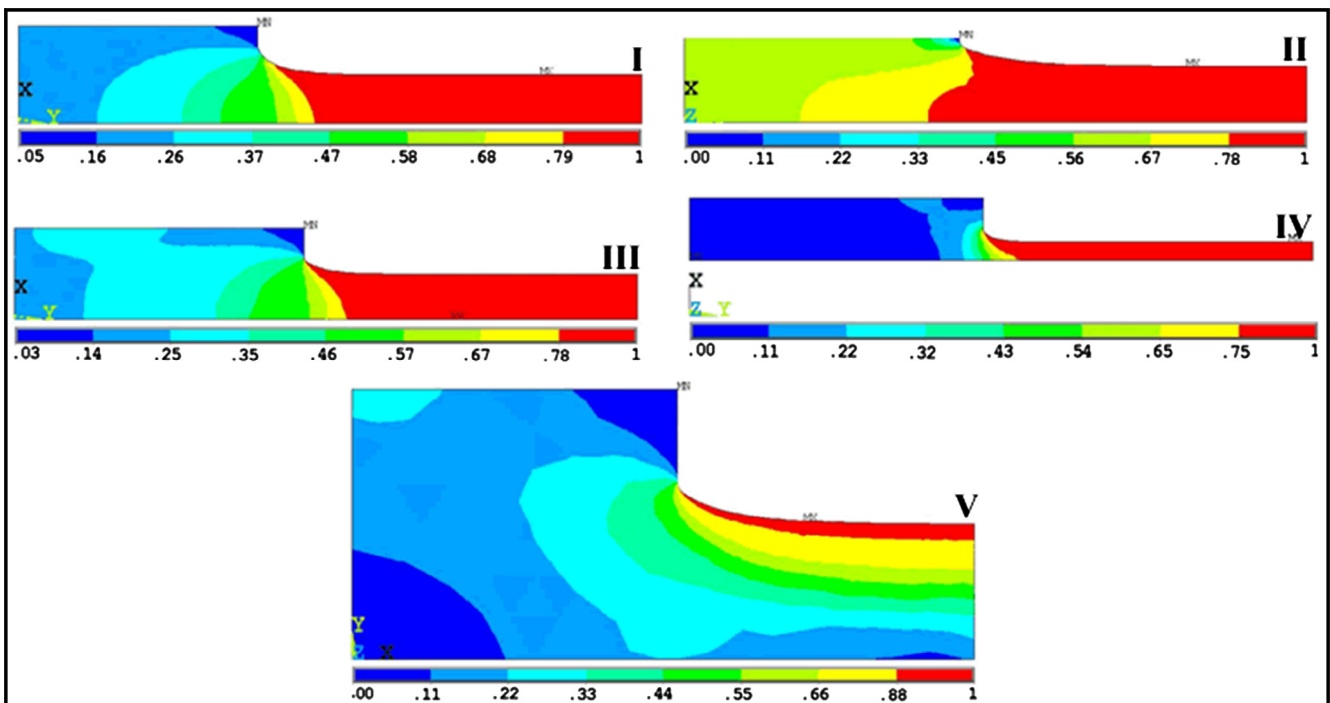


Fig. 18. Mises stress distribution around the variable radii fillets of the optimized fatigue TSs.

section to the larger heads needed to grip them, with generous radii that significantly decrease, but do not minimize their SCF. All such TSs were modeled in ANSYS APDL 12 assuming plane stress conditions and using triangular FE with six nodes and twelve degrees of freedom, but the schema depicted in Fig. 8 flow chart would work in any other FE code. Due to their symmetry conditions, only one quarter of the TS need to be modeled. TS type I and III are cylindrical and axisymmetric; type II has a rectangular symmetric section; type IV has a tubular profile axisymmetric about the y-axis; and type V has a rectangular profile anti-symmetric about the y-axis for its bending load conditions.

In particular, too many type V alternated-bending TSs with an original rounded notch tips were initiating fatigue cracks at their tip roots under actual test conditions, invalidating in this way

those tests results, a quite annoying problem partially due to the high notch-sensitivity of the tested high-strength steel. But after the notch tip profile of those specimens was optimized, this problem was completely eliminated and no other specimen broke near the notch root, a good illustration of how useful such procedures can be in real life.

Fig. 16 shows the original and the improved Mises stress plots along the notch profiles of the various fatigue test specimens studied here, calculated by FE models. Specimens type I–III already had very small SCF, but note how the original stress profile is variable along their circular arc tips, whereas the variable notch radii resulting from the gradient optimization process lead to a much more uniform stress distribution. On the other hand, specimen type IV, the standard shape for tension–torsion fatigue tests,

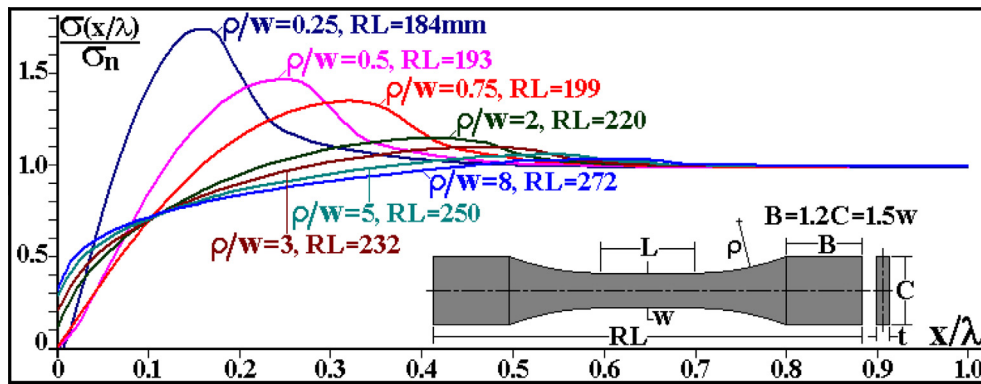


Fig. 19. Stress distribution along the boundary of circular arc shoulder fillets.

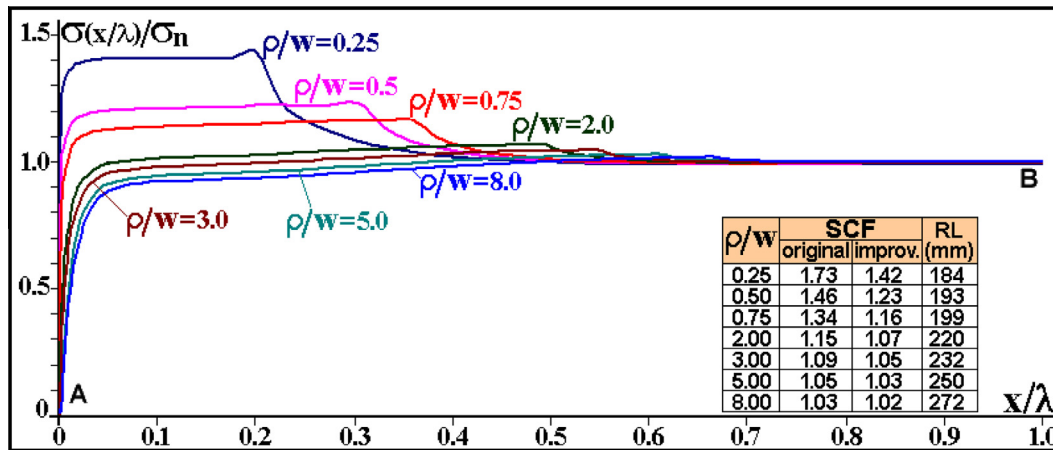


Fig. 20. Stress distribution along the boundary of the improved variable radii shoulder fillets, for various initially quarter-circular notch tips with  $0.25 \leq \rho/w \leq 8$ .

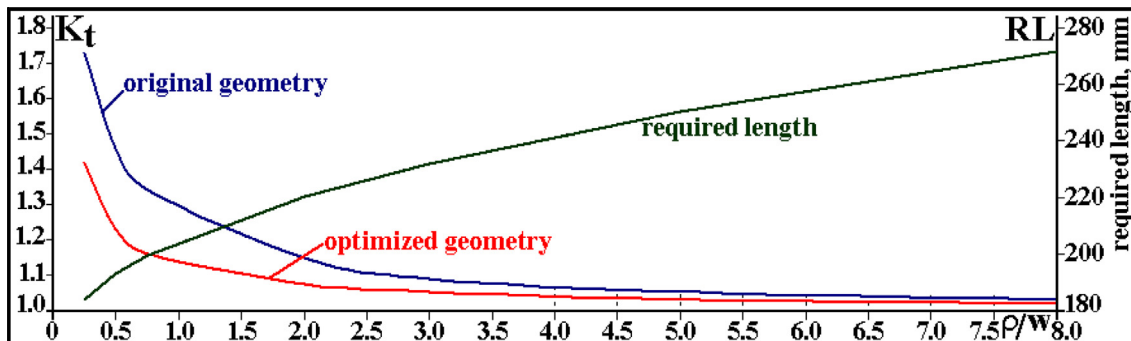


Fig. 21. SCF and required length of original and improved TS type II with originally circular arc.

originally had a surprisingly high  $K_t$  value, which was much improved by the optimization process. This improved shape is now being successfully used in the multiaxial fatigue tests made by our research group, see e.g. [33], so we can recommend it. This indicates that the ASTM tension–torsion standard should probably be reviewed. Moreover, the crack localization problem observed when testing standard TS type V was solved by this process.

Fig. 17 shows the final FE meshes automatically generated by this optimization process, and Fig. 18 shows the Mises stress distribution obtained along the entire optimized specimens (notice how uniform they turn out to be along the notch profile).

To better understand how a circular arc notch tip with a generous rounding radius compares with an optimized variable radii profile for reducing the SCF of a given TS, Fig. 19 compares 7 different circular arc shoulder fillets, in order to show how the  $\rho/w$  ratio affects the SCF of TS similar to the type II push–pull specimen shown in Fig. 15, but with a smaller  $C/w = 1.5$  ratio. As shown in Fig. 19, the SCF induced by a shoulder fillet with a relatively small circular arc with  $\rho/w = 0.25$  reaches a SCF value  $K_t \cong 1.8$ . As the  $\rho/w$  ratio increases, this  $K_t$  value reduces considerably, until it almost reaches a unit value when  $\rho/w \cong 8$ , which explains why ASTM specified this ratio as its standard fillet radius.

However, although traditional circular arc shoulder fillets may achieve quite low SCF values, they are far from the best choice. Indeed, assuming a fixed gage length, as the constant radius of the TS fillet increases, the required overall TS length (RL) also increases. Longer TS require more material, but their main problem is to be less buckle-resistant than shorter specimens with improved shoulders with equally low SCF values, a major problem in push–pull fatigue tests. When such limitations are important, both the gradientless and the gradient algorithms may be used with geometrical constraints, such as the given maximum length. Fig. 20 shows the stress distribution along the improved shoulders for the flat TS shown in Fig. 19, with  $C/w = 1.5$  and original (fixed)  $\rho/w$  ratios also ranging from 0.25 to 8. As expected, the notch optimization process is more efficient for reducing the high SCF of notches with low  $\rho/w$  ratios, since for high  $\rho/w$  values the initial SCF is already low to start with. However, even in such cases, the spline-based gradientless optimization algorithm leads to fillets with an almost uniform tangential stresses along their variable radii boundary.

To close this study, Fig. 21 compares the original and the improved TS type II SCFs for initial circular notches with  $0.25 \leq \rho/w \leq 8$ , as well as the required TS length  $RL$  as a function

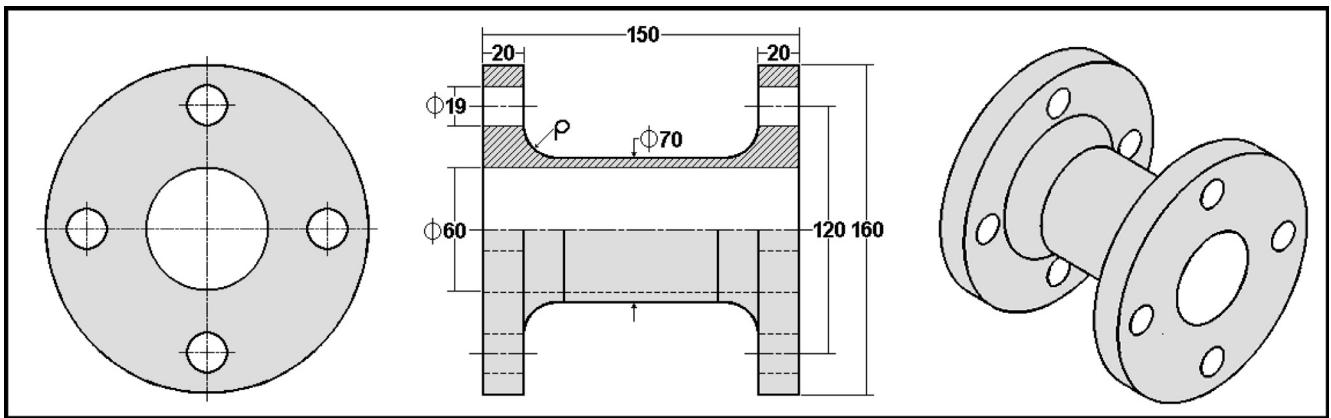


Fig. 22. Original load cell design, with a  $\rho = 75$  mm circular arc notch tip profile.

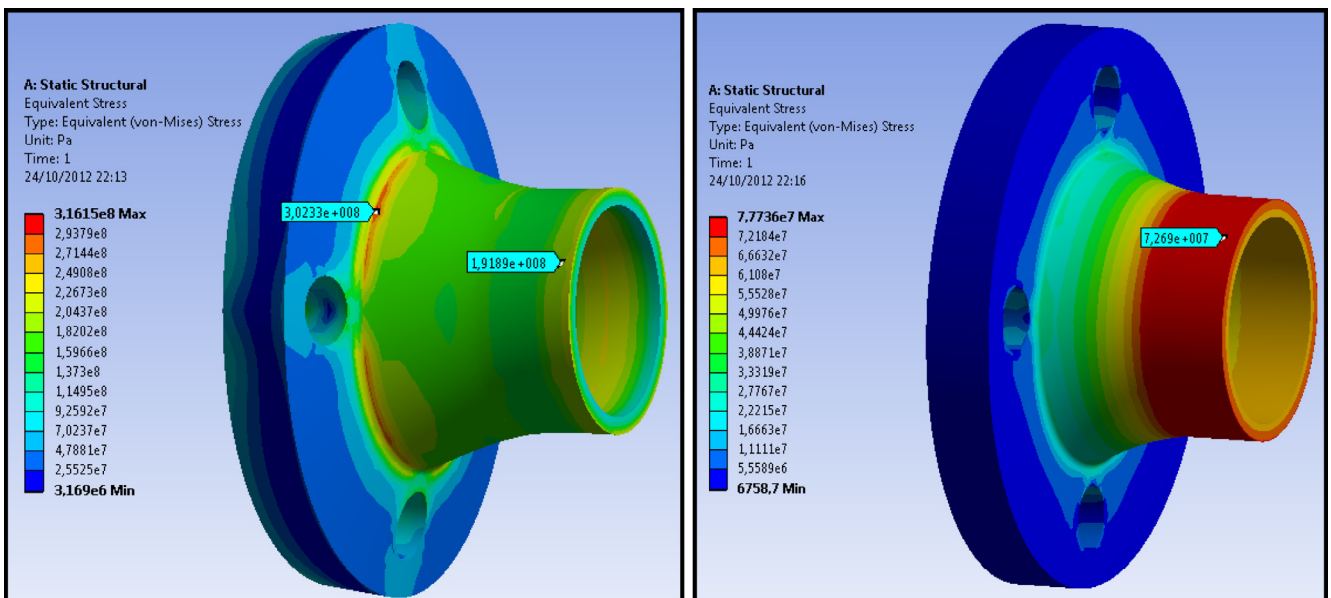


Fig. 23. Mises stress distribution along the original quart-circular notch profiles.

of the  $\rho/w$  ratio of the original TS. These optimization procedures may be particularly efficient if applied to similarly notched structural components when their  $\rho/w$  ratios are low due to space limitations, an important practical problem. In such cases, it may be more interesting or even mandatory to find an economical and feasible improved geometry for the new notch profile respecting the original space limitations, instead of searching for a globally optimum solution that would imply in a redesign of the entire component. Indeed, Fig. 21 shows that it is possible to find an improved fillet profile that leads to both a reduced SCF and to a smaller length for a TS type II with originally circular arc shoulder fillets. For example, for an initial circular arc fillet with  $\rho/w = 1.5$  the SCF of the improved shoulder reduces from  $K_t \cong 1.22$  to  $K_t \cong 1.1$  with a required TS length of  $RL \cong 215$  mm, whereas a circular arc shoulder fillet would require  $\rho/w \cong 2.6$  and  $RL \cong 228$  mm to achieve the same SCF value.

**5. Optimization of the fillets of a tension–torsion load cell**

Another practical application further illustrates the usefulness of the proposed spline-based gradientless notch optimization process: the design of a compact tubular tension–torsion load cell

schematized in Fig. 22. This load cell was designed to work in a custom-made electromechanical multiaxial axial–torsional fatigue testing machine under combined fatigue axial (push–pull) loads with amplitudes up to  $P = 200$  kN and torsion loads with amplitudes up to  $T = 1300$  N m. The load cell had a fixed axial size and was designed to measure the axial and the torsional loads using conventional strain gages wired in separated Wheatstone bridges. Its original design used large circular arc shoulder fillets with  $\rho = 75$  mm, but its FE analysis showed that although its torsion SCF was acceptable,  $K_{tT} = 1.07$ , despite this large notch tip radius its tension SCF was quite high,  $K_{tP} = 1.61$ . The stress distributions induced by the axial and by the torsional loads along the original notch tip profile are illustrated in Fig. 23. The problem with this original design is that the too high axial SCF value was leading to a relatively short fatigue crack initiation life within its required reliability, a certainly not acceptable feature for the application in question.

So, the very same spline-based gradient shape optimization procedure described above was used to reduce the SCFs of the tubular tension–torsion load cell fillets, maintaining its overall length. An axisymmetric model was created and the fillet profile was iteratively changed, according to the proposed algorithm. After

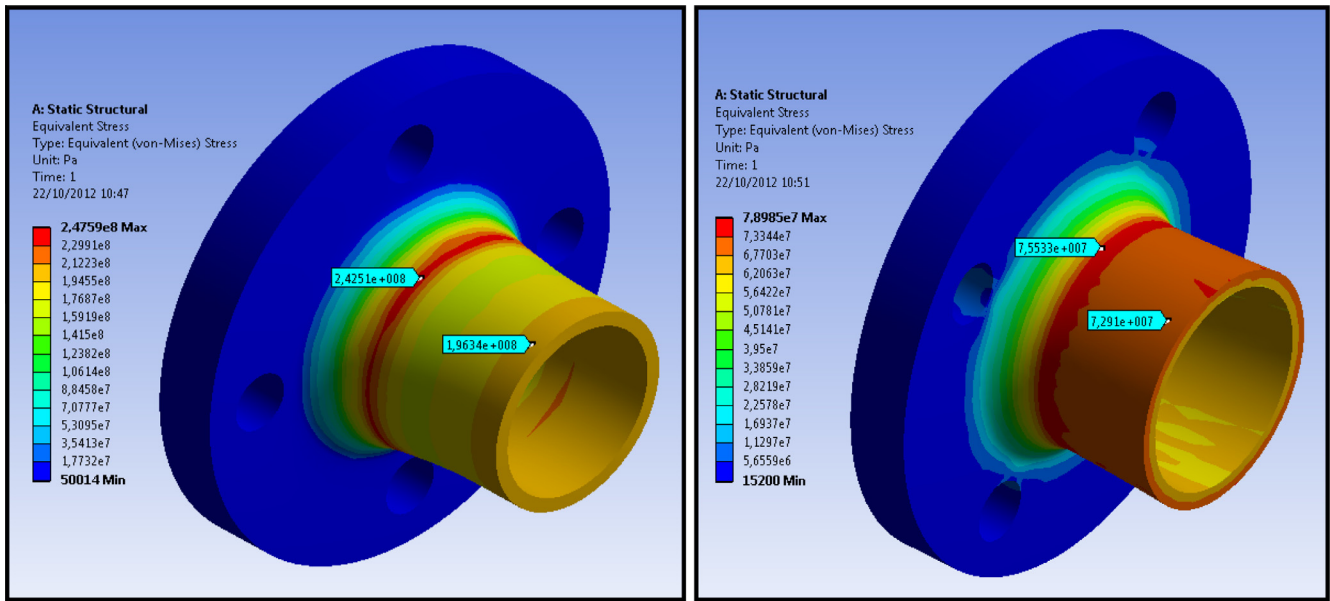


Fig. 24. Mises stress distribution along the improved load cell, with its notch profile optimized within the restriction of maintaining its overall length.

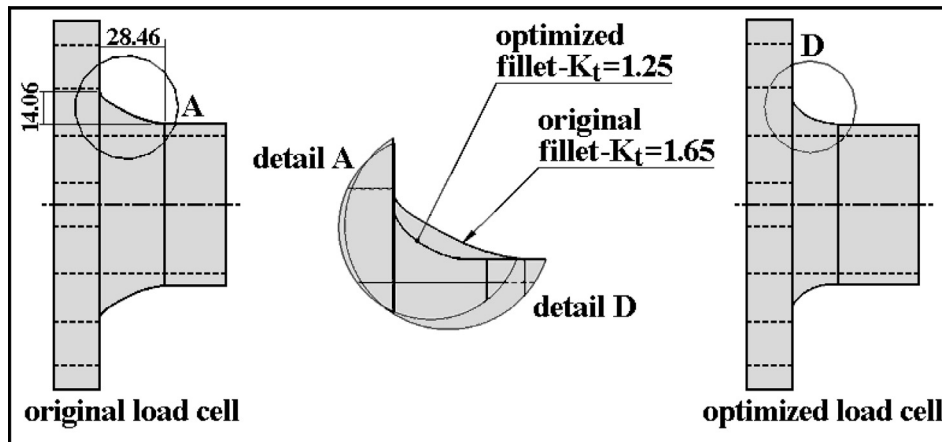


Fig. 25. Original and optimized fillets for the tubular tension–torsion load cell.

this shape iterative optimization process, the new fillet geometry reduced the tension SCF to  $K_{tp} = 1.23$  and the torsion one to  $K_{tT} = 1.035$ , solving the fatigue life problem without significantly increasing the tension–torsion load cell weight or even its cost, since it had to be machined on a CNC lathe anyway, see Fig. 24. The original and the optimized fillets are schematized in Fig. 25. Note that the optimized profile in fact reduced the material used in the fillet region, a non-intuitive result.

## 6. Conclusions

To maintain uniform tangential stress distributions along the notch tip boundaries is the way to minimize their stress concentration values, decreasing their deleterious effects that are especially prejudicial for fatigue applications. However, to obtain such uniform stress profiles it is necessary to design the notches with a variable tip profile, instead of the circular arc used in most engineering structures to smooth their notch tips. Following this idea, iterative SCF gradientless and gradient-based optimization algorithms were developed and implemented in a finite element environment. The basic idea of this optimization technique is to use splines to model any notch tip profile and iteratively change the position of the spline control points until the stress distribution is constant (or near constant), according to a prescribed numerical tolerance. This is a very efficient way of significantly improving the notch shapes by minimizing their SCF, a much useful feature especially suitable to improve the intrinsic fatigue resistance of structural components that must be designed with large section reductions or with size limitations. To show how useful this simple but powerful notch optimization algorithm can be in practice, it was applied to propose better profiles for standard fatigue test specimens, as well as to improve the design of a tension–torsion multiaxial load cell that had a length limit, which despite its large notch tip radii still was susceptible to fatigue failures, but it can equally be used with virtually any structural component.

## Acknowledgments

CNPq, the Brazilian Research Council has provided research scholarships for some of the authors, and ONR, the Office of Naval Research of the US Navy has provided a grant under the supervision of Dr. W. Nickerson to partially support this work.

## References

- [1] R.C.O. Góes, J.T.P. Castro, L.F. Martha, 3D effects around notch and crack tips, *Int. J. Fatigue* 62 (2014) 159–170.
- [2] J.T.P. Castro, M.A. Meggiolaro, *Fatigue Design Techniques*, volumes 1 and 2, CreateSpace 2016.
- [3] S. Timoshenko, J. Goodier, *Theory of Elasticity*, McGraw-Hill, 1969.
- [4] C.E. Inglis, Stress in a plate due to the presence of cracks and sharp corners, *Phil. Trans. R. Soc. A* 215 (1913) 119–233.
- [5] W. Pilkey, D. Pilkey, R. Peterson, *Peterson's Stress Concentration Factors*, John Wiley, 2008.
- [6] G.N. Savin, *Stress Distribution around Holes*, NASA Technical Translation, 1968, p. 10.
- [7] J.T.P. Castro, R.V. Landim, J.C.C. Leite, M.A. Meggiolaro, Prediction of notch sensitivity effects in fatigue and EAC, *Fatigue Fract. Eng. Mater. Struct.* 38 (2) (2015) 161–179.
- [8] J.T.P. Castro, M.A. Meggiolaro, A.C.O. Miranda, H. Wu, A. Imad, B. Nouredine, Prediction of fatigue crack initiation lives at elongated notch roots using short crack concepts, *Int. J. Fatigue* 42 (2012) 172–182.
- [9] ASTM E 606 – 92: Standard Practice for Strain-Controlled Fatigue Testing, Annual Book of ASTM Standards, ASTM 1993.
- [10] ASTM E 2207 – 02: Standard Practice for Strain-Controlled Axial-Torsional Fatigue Testing with Thin-Walled Tubular Specimens, Annual Book of ASTM Standards, West Conshohocken, PA, 2002.
- [11] ASTM E 606 – 92: Standard Practice for Controlled Constant Amplitude Axial Fatigue Test of Metallic Materials, Annual Book of ASTM Standards, West Conshohocken, PA, 2002.
- [12] M. Garrell, A. Shih, E.L. Curzio, R. Scattergood, Finite element analysis of stress concentration in ASTM D 638 tension specimens, *J. Testing Eval.* 31 (1) (2003) 52–57.
- [13] R. Lansard, Fillets without stress concentration, *Laboratories de la Société des Automobiles Peugeot* (1954).
- [14] R.B. Heywood, *Photoelasticity for Designers*, Pergamon, 1969.
- [15] C. Mattheck, *Design in Nature: Learning from Trees*, Springer, 1998.
- [16] C. Mattheck, Teacher tree: the evolution of notch shape optimization from complex to simple, *Eng. Fract. Mech.* 73 (12) (2006) 1732–1742.
- [17] C. Mattheck, S. Burkhardt, A new method of structural shape optimization based on biological growth, *Int. J. Fatigue* 12 (3) (1990) 185–190.
- [18] F.O. Sonmez, Shape optimization of 2D structures using simulated annealing, *Comput. Methods Appl. Mech. Eng.* (2007) 3279–3299.
- [19] F.O. Sonmez, Optimal shape design of shoulder fillets for flat and round bars under various loadings, *Proc. J. Mech. Eng. Sci.* 223 (C8) (2009) 1741–1754.
- [20] F.O. Sonmez, Structural optimization using simulated annealing, in: *Simulated Annealing*, I-Tech Education and Publishing, 2008.
- [21] R. Das, R. Jones, Y.M. Xie, Design of structures for optimal static strength using ESO, *Eng. Failure Anal.* 12 (2005) 61–80.
- [22] E. Schnack, An optimization procedure for stress concentration by the finite element technique, *Int. J. Numer. Methods Eng.* 14 (1979) 115–124.
- [23] G. Meneghetti, C. Guzzella, B. Atzori, The peak stress method combined with 3D finite element models for fatigue assessment of toe and root cracking in steel welded joints subjected to axial of bending loading, *Fatigue Fract. Eng. Mater. Struct.* 37 (2014) 722–739.
- [24] M. Heller, R. Kaye, L.R.F. Rose, A gradientless finite element procedure for shape optimization, *J. Strain Anal.* 34 (5) (1999) 323–336.
- [25] W. Waldman, M. Heller, G.X. Chen, Optimal free-form shapes for shoulder fillet in flat plates under tension and bending, *Int. J. Fatigue* 23 (6) (2000) 509–523.
- [26] Z. Wu, On the optimization problem of fillets and holes in plates with curvatures constraints, *Struct. Multidiscip. Opt.* 35 (5) (2008) 499–506.
- [27] Z. Wu, An efficient approach for shape optimization of components, *Int. J. Mech. Sci.* 47 (10) (2003) 1595–1610.
- [28] P. Pedersen, C.L. Laursen, Design for minimum stress concentration by finite elements and linear programming, *J. Struct. Mech.* 10 (1982–1983) 243–271.
- [29] R. Kaye, M. Heller, Investigation of shape optimization for the design of life extension options for an F/A-18 airframe FS 470 bulkhead, *J. Strain Anal. Eng. Des.* 35 (6) (2000) 493–505.
- [30] R.C. Carbonari, P.A. Muñoz-Rojas, E.Q. Andrade, G.H. Paulino, K. Nishimoto, E.C. N. Silva, Design of pressure vessels using shape optimization: an integrated approach, *Int. J. Press. Vessels Pip.* 88 (2011) 198–212.
- [31] G.N. Vanderplaats, *Numerical Optimization Techniques for Engineering Design*, McGraw-Hill, 1984.
- [32] N. Karmarkar, A new polynomial-time algorithm for linear programming, *Combinatorica* 4 (4) (1984) 373–395.
- [33] H. Wu, M.A. Meggiolaro, J.T.P. Castro, Validation of the multiaxial racetrack amplitude filter, *Int. J. Fatigue* (2016) (in press), <http://dx.doi.org/10.1016/j.ijfatigue.2016.01.016>.